General formula to design a freeform singlet free of spherical aberration and astigmatism

Article *in* Applied Optics · January 2019

DOI: 10.1364/AO.58.001010

CITATIONS
42

READS
8,697

3 authors:

Rafael G. González-Acuña
Huawei Technologies
136 PUBLICATIONS **466** CITATIONS
SEE PROFILE

Hector Alejandro Chaparro Romo
Independient
56 PUBLICATIONS **237** CITATIONS
SEE PROFILE

Julio Cesar Gutierrez Vega
Tecnológico de Monterrey
273 PUBLICATIONS **6,308** CITATIONS
SEE PROFILE

applied optics

General formula to design a freeform singlet free of spherical aberration and astigmatism

Rafael G. González-Acuña,[1,*] Héctor A. Chaparro-Romo,[2] and Julio C. Gutiérrez-Vega[1]

[1]Photonics and Mathematical Optics Group, Tecnológico de Monterrey, Monterrey 64849, Mexico
[2]UNAM, Av. Universidad 3000, Cd. Universitaria, Coyoacán, 04510 Ciudad de México, Mexico
*Corresponding author: rafael123.90@hotmail.com

Received 9 November 2018; revised 17 December 2018; accepted 18 December 2018; posted 19 December 2018 (Doc. ID 351567); published 29 January 2019

In this paper, an analytical closed-form formula for the design of freeform lenses free of spherical aberration and astigmatism is presented. Given the equation of the freeform input surface, the formula gives the equation of the second surface to correct the spherical aberration. The derivation is based on the formal application of the variational Fermat principle under the standard geometrical optics approximation.

https://doi.org/10.1364/AO.58.001010

1. INTRODUCTION

Freeform optics involves the design of optical elements with at least one surface that has no translational or rotational symmetry with respect to a propagation axis. In recent years, the topic has gained increasing popularity in the optics community, partly because of the rapid development of new computing technologies and the emergence of potential applications. In general, the design of freeform elements has combined theoretical approximation methods with brute-force optimization techniques, leading to a diversity of results and methodologies that have proved to be useful for particular cases [1,2]. For instance, Forbes [3–6] described freeform surfaces based on a set of characteristic polynomials for non-rotationally symmetric systems. Recently, the generation of freeform mirrors have been studied [7,8], which considerably reduces the optical aberrations. The theory of aberration of freeform optics has been developed by several authors [9–12] applying numerical optimization schemes. More recently, with the simultaneous multiple surfaces method, interesting solutions for several cases of freeform and radially symmetric cases employing numerical approaches based on general Cartesian ovals have been reported [13–18]. The general Cartesian ovals problem was first considered by Levi-Civita in 1900, without giving an analytical closed-form formula [19]. The generalized Cartesian oval problem consists of finding a refractive surface that transforms a given incoming wavefront into another given outgoing wavefront.

In this paper, we address the case when one of the wavefronts is freeform and the other one is spherical. The freeform wavefront is generated by the first surface of the lens, and the spherical wavefront is generated by the second surface. Further, we introduce a closed-form expression for the design of freeform singlets lenses free of spherical aberration and astigmatism, which can be considered as a continuation of our work [20,21]. The formula gives the exact analytical equation of the output surface, given the arbitrary freeform expression of the input surface to correct the spherical aberration and the astigmatism introduced by the first surface. The derivation is fully analytically based on the formal application of the variational Fermat principle under the standard geometrical optics approximation. In the process of deriving the formula, we apply a design methodology free of numerical optimization strategies. We illustrate the applicability and robustness of the formula by showing some representative design examples using very sophisticated input functions that have not been used before in optical design. To the best of our knowledge, this exact formula has not been reported before in the optical design literature.

2. ANALYTICAL DESIGN OF A FREEFORM SINGLET FREE OF SPHERICAL ABERRATION

We assume that the singlet lens is a lossless and homogeneous optical element with the relative refractive index n and axial thickness T (see Fig. 1). Its input surface is known, and it is described by the freeform function $z_a(x_a, y_a)$, where the subindex a refers to the coordinates on the input surface. The shape of the output surface is unknown, and it is described by the function $z_b(x_b, y_b)$, which is to be determined, where the subindex b refers to the coordinates on the output surface. We will further assume that the normal vector of the input surface at the optical axis points out in the direction z, that is, the normal is perpendicular to the tangent plane of the input surface at the origin.

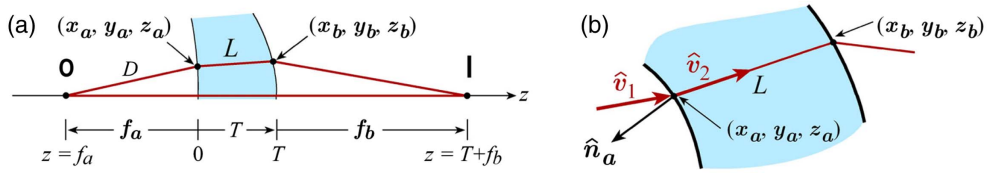

Fig. 1. (a) Geometry of the problem and notation used for the distances. The origin of the coordinate system is located at the center of the input surface $z_a(0,0) = 0$. (b) Zoom showing the notation for the unit vectors.

The goal is to determine the output function $z_b(x_b, y_b)$ given the input function $z_a(x_a, y_a)$ to correct the spherical aberration introduced by the first surface. To do this, we will consider an object point (O) located at $z = f_a$ on the optical axis and its corresponding image point (I) focused at $z = T + f_b$, as shown in Fig. 1(a). The input field impinging on the freeform singlet is a monochromatic spherical wave emerging from the source (O). Since the size of the freeform singlet is much larger than the wavelength of the light, a ray optics representation may be applied to solve this problem. In this approach, the input field is characterized by a uniform bundle of radial rays emerging from (O).

We begin by recalling the Snell law in the vector form for an incident ray coming from medium n_1 and transmitted to medium n_2 [22]:

$$n\hat{\mathbf{v}}_2 = [\hat{\mathbf{n}}_a \times (-\hat{\mathbf{n}}_a \times \hat{\mathbf{v}}_1)] - \hat{\mathbf{n}}_a \sqrt{n^2 - (\hat{\mathbf{n}}_a \times \hat{\mathbf{v}}_1) \cdot (\hat{\mathbf{n}}_a \times \hat{\mathbf{v}}_1)}, \tag{1}$$

where $n = n_2/n_1$ is the relative refractive index, $\hat{\mathbf{n}}_a$ is the normal unit vector of the input surface pointing toward the incident medium, and $\hat{\mathbf{v}}_1$ and $\hat{\mathbf{v}}_2$ are the propagation unit vectors of the incident and refracted rays, respectively [see Fig. 1(b)]. If the ray strikes the input surface at the point (x_a, y_a, z_a) and emerges from the lens at (x_b, y_b, z_b), then the unit vectors can be expressed as

$$\hat{\mathbf{n}}_a = \frac{[z_{a_x}, z_{a_y}, -1]}{S}, \qquad \hat{\mathbf{v}}_1 = \frac{[x_a, y_a, z_a - f_a]}{D}, \qquad \hat{\mathbf{v}}_2 = \frac{[x_b - x_a, y_b - y_a, z_b - z_a]}{L}, \tag{2}$$

where

$$S \equiv \sqrt{z_{a_x}^2 + z_{a_y}^2 + 1}, \qquad D \equiv \sqrt{x_a^2 + y_a^2 + (z_a - f_a)^2}, \qquad L \equiv \sqrt{(x_b - x_a)^2 + (y_b - y_a)^2 + (z_b - z_a)^2}, \tag{3}$$

and $z_{a_x} \equiv \partial_x z_a$ and $z_{a_y} \equiv \partial_y z_a$ are the partial derivatives of $z_a(x_a, y_a)$ with respect to x_a and y_a. Note that S and D depend on the input surface exclusively, whereas L depends on both the input and output surfaces.

Replacing the unit vectors Eq. (2) into the vector Eq. (1) and separating the Cartesian components, we get the following expressions for the direction cosines X, Y, and Z of the vector $\hat{\mathbf{v}}_2$:

$$\mathcal{X} \equiv \frac{x_b - x_a}{L} = \frac{x_a(z_{a_y}^2 + 1) - z_{a_x}(y_a z_{a_y} + f_a - z_a)}{nDS^2} - z_{a_x}\frac{\Phi}{S}, \tag{4a}$$

$$\mathcal{Y} \equiv \frac{y_b - y_a}{L} = \frac{y_a(z_{a_x}^2 + 1) - z_{a_y}(x_a z_{a_x} + f_a - z_a)}{nDS^2} - z_{a_y}\frac{\Phi}{S}, \tag{4b}$$

$$\mathcal{Z} \equiv \frac{z_b - z_a}{L} = \frac{(z_a - f_a)(z_{a_x}^2 + z_{a_y}^2) + x_a z_{a_x} + y_a z_{a_y}}{nDS^2} + \frac{\Phi}{S}, \tag{4c}$$

where

$$\Phi \equiv \left[1 - \frac{(y_a z_{a_x} - x_a z_{a_y})^2 + [z_{a_x}(z_a - f_a) + x_a]^2 + [z_{a_y}(z_a - f_a) + y_a]^2}{n^2 D^2 S^2}\right]^{1/2}, \tag{5}$$

and, evidently, $\mathcal{X}^2 + \mathcal{Y}^2 + \mathcal{Z}^2 = 1$. Relations (4) come from the application of the Snell law for an arbitrary ray striking the singlet lens at the point (x_a, y_a, z_a). Note that the expressions in the right sides of Eq. (4) are fully expressed in terms of the coordinates of the input surface, that is, $\mathcal{X} = \mathcal{X}(x_a, y_a, z_a)$ and so on.

We will now derive an additional relation to fulfill the free spherical aberration condition. Let us consider two rays emerging simultaneously from (O): the first one strikes the singlet at (x_a, y_a, z_a), and the second one travels along the optical axis [see Fig. 1(a)]. Both rays pass through the singlet and meet again at the image point (I) located at $(0, 0, T + f_b)$. The Fermat principle requires that both optical lengths between the points (O) and (I) be the same. Thus, equating the optical paths, we get

$$-f_a + nT + f_b = -\mathrm{sgn}(f_a)D + nL + \mathrm{sgn}(f_b)\sqrt{x_b^2 + y_b^2 + (z_b - T - f_b)^2}, \tag{6}$$

where sgn(•) is the sign function. For negative (positive) values of f_a, the object is real (virtual), and for positive (negative) values of f_b, the image is real (virtual).

Equations (4) and (6) form a system of algebraic equations for the unknowns x_b, y_b, and z_b, whose exact solution is given by

$$x_b = x_a + \frac{\mathcal{X}(z_b - z_a)}{\mathcal{Z}}, \qquad y_b = y_a + \frac{\mathcal{Y}(z_b - z_a)}{\mathcal{Z}}, \qquad z_b = \frac{g - \sqrt{g^2 + h(n^2 - 1)}}{n^2 - 1}, \tag{7}$$

where

$$g \equiv (z_a - f_b - T)\mathcal{Z}^2 + q\mathcal{Z} + z_a(n^2 - 1), \tag{8a}$$

$$h \equiv [x_a^2 + y_a^2 - z_a^2 + (T + f_b)^2 - (p - nT)^2]\mathcal{Z}^2 - 2z_a q\mathcal{Z} - z_a^2(n^2 - 1), \tag{8b}$$

$$p \equiv -\mathrm{sgn}(f_a)D + f_a - f_b, \tag{8c}$$

$$q \equiv x_a\mathcal{X} + y_a\mathcal{Y} - np + n^2 T. \tag{8d}$$

Equations under (7) are the most important result of this paper. They describe analytically the shape $z_b(x_b, y_b)$ of the output surface of the singlet lens in terms of the function $z_a(x_a, y_a)$ of its freeform input surface and the design parameters (f_a, f_b, n, T). These equations may look cumbersome, but it is quite remarkable that they could be expressed in closed form for an arbitrary freeform input surface. To the best of our knowledge, these relations have not been derived before. We recall that a necessary condition for the validity of Eq. (7) is that the surface normal should be perpendicular to the tangent plane to the input surface at the origin.

From a more mathematical point of view, since the freeform lens is a homogeneous optical element, the input and output surfaces are simple connected sets on $\mathbb{R}^3$ that can be defined as

$$\Psi_a = \{(x_a, y_a, z_a) \in \mathbb{R}^3 | z_a < z_b\}, \qquad \Psi_b = \{(x_b, y_a, z_b) \in \mathbb{R}^3 | z_b > z_a\}, \tag{9}$$

where Ψ_a and Ψ_b are homeomorphic, which means that both surfaces are topologically equivalent. Thus, there exists a continuous and bijective function f such that $f{:}\Psi_a \to \Psi_b$, and whose inverse f^{-1} is also continuous. There are many functions f that map both sets, but there is only one that is physically valid and corresponds to that one that satisfies the variational Fermat principle of minimum optical length. In our case, it is clear that f is given by Eq. (7). The uniqueness of f has as a consequence that the Snell law is automatically fulfilled at the second interface z_b as well. Now, since f is continuous, it means that f maps open balls from Ψ_a to Ψ_b, and then the ray neighborhoods are preserved. Therefore, the validity of Eq. (7) also requires that the rays do not intersect each other inside the lens because, in this case, Ψ_b overlaps itself, leaving from being homeomorphic with respect to Ψ_a, and the vicinity of the neighborhoods is not preserved.

3. ILLUSTRATION OF RELEVANT EXAMPLES

The generality of Eq. (7) allows us to show a large variety of interesting geometries of the singlet lens. In all examples, the input surface is freeform, and it is defined by the user.

Let us begin by considering a non-circularly symmetric convex surface described by the elliptical paraboloid $z_a = (x_a^2 + 8y_a^2)/200$ shown in Fig. 2(a). The output surface $z_b(x_b, y_b)$ was calculated evaluating directly Eq. (7) using the design parameters included in the caption of the figure. In this case, the output function resembles a hyperbolic paraboloid. The border of the singlet is a three-dimensional curve $\mathbf{r}_{\mathrm{border}}$ that can be determined by the intersection of the input and output surfaces, that is, $z_a(\mathbf{r}_{\mathrm{border}}) = z_b(\mathbf{r}_{\mathrm{border}})$. Unfortunately, it seems that there is not a close-form analytical expression for the border, but it can be calculated numerically finding the intersection of both surfaces. Evidently, the size of the lens increases as the thickness T increases. Figure 2(a) also shows the trajectories for a set of rays emerging from the source (O) and converging to the image (I). For visualization purposes, we have drawn a cut of the lens as if it were hollow to appreciate clearly the surfaces and the internal trajectories of the rays.

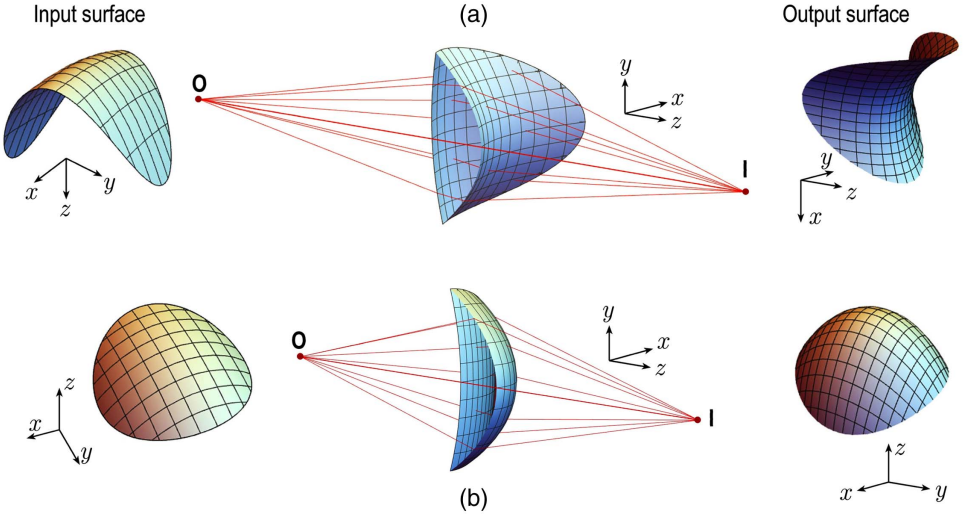

Fig. 2. Singlet lenses with non-uniform (a) convex and (b) concave input surfaces with $n = 1.5$, $T = 1$ cm, $f_a = -5$ cm, and $f_b = 6$ cm.

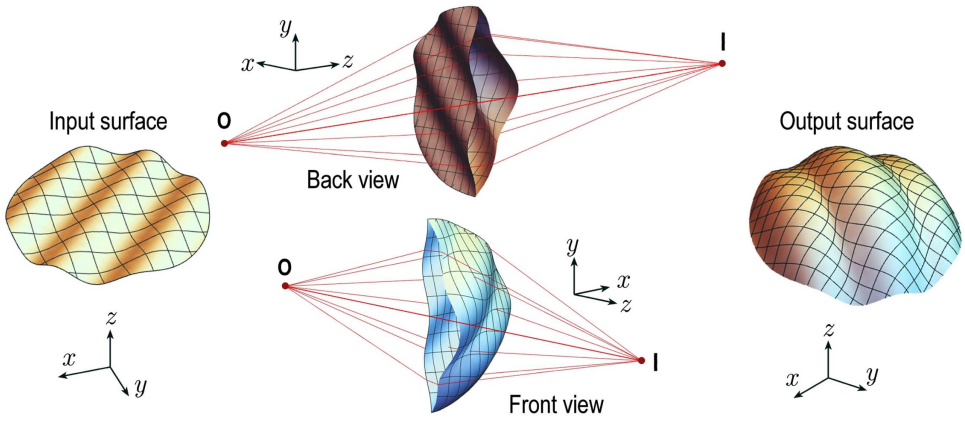

Fig. 3. Singlet lens with sinusoidal input surfaces with $n = 1.5$, $T = 1$ cm, $f_a = -5$ cm, and $f_b = 6$ cm. Please see Visualization 1.

In Fig. 2(b), we illustrate the case of a concave surface described by the ellipsoid $z_a = -50 + (50^2 - x_a^2 - 3y_a^2)^{1/2}$.

Figure 2 shows examples of simple concave and convex input surfaces, but Eq. (7) can be evaluated using more challenging input functions combining concave and convex regions. In Fig. 3, we show a singlet with a harmonic sinusoidal input surface given by $z_a = \cos(0.4x_a + 0.4y_a)$. Except for the shape of the input function, all remaining parameters are the same as in Fig. 2. The spatial frequency of the input function modulating the input surface can be increased until the limit when the rays propagating inside the glass intersect each other. We show the back and front views to facilitate the visualization of the rays traveling from (O) to (I).

In Fig. 4, we include three additional examples of freeform lenses. In the first two subplots, we illustrate the mixed behavior of convex functions with oscillating functions modulating the input surface: (a) $z_a = (x^2 \cos x + 8y^2)/200$, and (b) $z_a = [0.1 \cos y_a(y_a^2 + 16x_a^2)]/200$. From the figures, it is clear that the output rays converge to the image point despite the ripples of the input surfaces. Finally, we remark that the positions of the object f_a and the image f_b can be set to any value on the optical axis including the infinity. To show this case, in Fig. 4(c), we plot

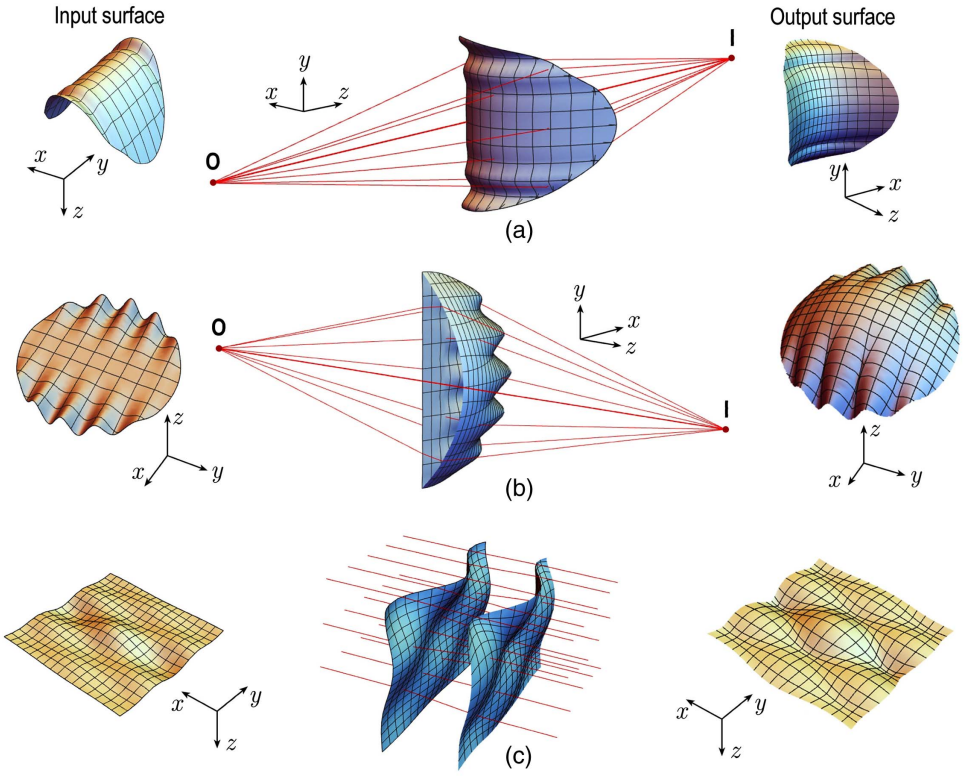

Fig. 4. Singlet lenses with input surfaces mixing concave/convex with oscillating behavior. Parameters $n = 1.5$ and $T = 1$ cm. Subplots (a) and (b) with $f_a = -5$ cm and $f_b = 6$ cm. Subplot (c) $f_a \to -\infty$ and $f_b \to \infty$. See Visualization 2 for the subplot (a).

the ray tracing for the input surface $z_a = -J_0(x_a)\cos(0.45y_a)$ when the object is located at $-\infty$ and the image at ∞. We can see that the collimated input rays keep collimated after passing the lens, but with a different distribution. Thus, this device may be considered as a shaper of collimated beams.

A. Efficiency

To validate the efficiency of the Eq. (7), we compare the rays coming from the image and the rays that go to the image, so we have the following vectors $\boldsymbol{v}_3$ and $\boldsymbol{v}_3^{\dagger}$, $-\boldsymbol{v}_3$ comes from the image to the second surface, $\boldsymbol{v}_3^{\dagger}$ is computed using the Snell law at the second surface, and $\boldsymbol{n}_b$ is unitary the normal vector of the second surface. Therefore, $\boldsymbol{n}_b$, $\boldsymbol{v}_3$, and $\boldsymbol{v}_3^{\dagger}$ are written as

$$\begin{cases} \boldsymbol{n}_b = \pm \dfrac{\frac{\partial}{\partial x_a}[x_b, y_b, z_b] \times \frac{\partial}{\partial y_a}[x_b, y_b, z_b]}{\left|\frac{\partial}{\partial x_a}[x_b, y_b, z_b] \times \frac{\partial}{\partial y_a}[x_b, y_b, z_b]\right|}, \\ \boldsymbol{v}_3 = \dfrac{[x_b, y_b, z_b - T - f_b]}{\sqrt{x_b^2 + y_b^2 + (z_b - T - f_b)^2}}, \\ \boldsymbol{v}_3^{\dagger} = n[\boldsymbol{n}_b \times (-\boldsymbol{n}_b \times \boldsymbol{v}_2)] - \boldsymbol{n}_b \sqrt{1 - n^2(\boldsymbol{n}_b \times \boldsymbol{v}_2) \cdot (\boldsymbol{n}_b \times \boldsymbol{v}_2)}. \end{cases} \tag{10}$$

The percentage efficiency of the ray is measured in terms of how close it ends in the image position. Therefore, we defined the efficiency as

$$E = 100\% - \left|\frac{\boldsymbol{v}_3^{\dagger} - \boldsymbol{v}_3}{\boldsymbol{v}_3}\right| \times 100\%. \tag{11}$$

We compute the efficiency for 500 rays for all the examples presented in the paper, and the average of all the examples is 99.9999999999941′% ≈100%. We believe that the error is not zero because there are computational errors, such as truncation, that cannot be avoided.

Please note that all examples of the singlets are free of spherical aberration, even when the incident angles are very large. This happens because we do not use any paraxial approximation.

We have tested a large variety of input surfaces exhibiting exotic shapes and different spatial variations. In all cases, Eq. (7) gave the correct and expected behavior, provided that the rays traveling inside the freeform collimator lens do not self-intersect.

4. CONCLUSIONS

In this paper, we introduced a general Eq. (7) to design a singlet freeform lens free of spherical aberration and astigmatism. The method works as follows: for a given input surface (x_a, y_a, z_a), the formula yields a second surface (x_b, y_b, z_b) that corrects the spherical aberration generated by the first surface. We have tested many singlets with input surfaces exhibiting exotic shapes and different spatial variations for a variety of focal distances. In all cases, Eq. (7) gave the expected behavior, provided that the rays traveling inside the freeform lens do not cross each other. In this work, we have focused on eliminating the spherical aberration, but the optical systems exhibit more aberrations that we have not studied. Nevertheless, we are convinced that this family of freeform lenses has many potential applications. Also, it is important to mention that since Eq. (7) in general is not radially symmetric and is not a circle in the x–y, it also eliminates the astigmatism. Finally, we show the Mathematica code (see Code 1, Ref. [23]) to plot Eq. (7) in Appendix A.

APPENDIX A

We share the program code in the Mathematica language to plot freeform surfaces free of spherical aberration. The program has three sections: the first one declares Eq. (7); the second defines the constants of the optical system; and finally, in the third one, the plot is computed.

General formula to design freeform singlet free of spherical aberration and astigmatism

```
(* Clean register. *)
Clear["Global'*"]

(* freeform *)
za[xa_,ya_]:=Module[{q},q=Cos[0.4 xa]Cos[0.4 ya]]
e=10^(-5);
dxza[xa_,ya_]:=Module[{q},q=(za[xa+e,ya]-za[xa,ya])/e];
dyza[xa_,ya_]:=Module[{q},q=(za[xa,ya+e]-za[xa,ya])/e];
S[xa_,ya_]:=Module[{q},q=Sqrt[1+dxza[xa,ya]^2+dyza[xa,ya]^2]];
Di[xa_,ya_]:=Module[{q},q=Sqrt[xa^2+ya^2+(-fa+za[xa,ya])^2]];
L[xa_,ya_]:=Module[{q},q=Sqrt[(-xa+xb[xa,ya])^2+(-xa+yb[xa,
ya])^2+(-xa+zb[xa,ya])^2]]
\[CapitalPhi][xa_,ya_]:=Module[{q},q=\[Sqrt](1-((ya dxza[xa,
ya]-xa dyza[xa,ya])^2+(xa+dxza[xa,ya] (-fa+za[xa,ya]))^2+(ya
+dyza[xa,ya] (-fa+za[xa,ya]))^2)/(n^2 Di[xa,ya]^2 S[xa,ya]^2))]
X[xa_,ya_]:=Module[{q},q=(xa (1+dyza[xa,ya]^2)-dxza[xa,ya] (fa
+ya dyza[xa,ya]-za[xa,ya]))/(n Di[xa,ya] S[xa,ya]^2)-(dxza[xa,ya]
\[CapitalPhi][xa,ya])/S[xa,ya]]
Y[xa_,ya_]:=Module[{q},q=(ya (1+dxza[xa,ya]^2)-dyza[xa,ya] (fa
+xa dxza[xa,ya]-za[xa,ya]))/(n Di[xa,ya] S[xa,ya]^2)-(dyza[xa,ya]
\[CapitalPhi][xa,ya])/S[xa,ya]]
Z[xa_,ya_]:=Module[{q},q=(xa dxza[xa,ya]+ya dyza[xa,ya]+(dxza
[xa,ya]^2+dyza[xa,ya]^2) (-fa+za[xa,ya]))/(n Di[xa,ya] S[xa,ya]^2)
+\[CapitalPhi][xa,ya]/S[xa,ya]]
p[xa_,ya_]:=Module[{ww},ww=-Sign[fa]Di[xa,ya]+fa-fb]
q[xa_,ya_]:=Module[{ww},ww=n^2 T-n p[xa,ya]+xa X[xa,ya]+ya
Y[xa,ya]]
g[xa_,ya_]:=Module[{ww},ww=q[xa,ya] Z[xa,ya]+(-1+n^2) za[xa,
ya]+Z[xa,ya]^2 (-fb-T+za[xa,ya])]
h[xa_,ya_]:=Module[{ww},ww=(-n^2+X[xa,ya]^2+Y[xa,ya]^2) za
[xa,ya]^2-2 (n^2 t-n p[xa,ya]+xa X[xa,ya]+ya Y[xa,ya]) za[xa,ya]
Z[xa,ya]+((t+tb)^2+xa^2+ya^2-(-n t+p[xa,ya])^2) Z[xa,ya]^2]
zb[xa_,ya_]:=Module[{ww},ww=(g[xa,ya]-Sqrt[g[xa,ya]^2+(-1
+n^2) h[xa,ya]])/(-1+n^2)]
xb[xa_,ya_]:=Module[{ww},ww=xa+(X[xa,ya] (-za[xa,ya]+zb[xa,
ya]))/Z[xa,ya]]
yb[xa_,ya_]:=Module[{ww},ww=ya+(Y[xa,ya] (-za[xa,ya]+zb[xa,
ya]))/Z[xa,ya]]

(* constants of the optical system *)
n = 1.5; fa = -50; fb = 60; T = 10; s1 = -1; rmax = 20;

(* Plot *)
g0=ParametricPlot3D[{xb[x,y],yb[x,y],zb[x,y]},{x,-rmax,rmax},{y,-
rmax,rmax},RegionFunction->Function[{x,y},zb[x,y]>za[x,y]],
Axes->False,Boxed->False,PlotStyle->LightBlue,AxesLabel->{x,
y,z}];
g1=Plot3D[za[x,y],{x,-rmax,rmax},{y,-rmax,rmax},
RegionFunction->Function[{x,y},za[x,y]<zb[x,y]],PlotStyle-
>LightGray,Axes->False,Mesh->8, Boxed->False,BoxRatios-
>Automatic,AxesLabel->{x,y,z}];
Show[g0,g1,Boxed->False,PlotRange->All]
```

Funding. Consejo Nacional de Ciencia y Tecnología (CONACYT) (593740); Instituto Tecnológico y de Estudios Superiores de Monterrey (ITESM) (0020209I07).

REFERENCES

1. A. Bauer, E. M. Schiesser, and J. P. Rolland, "Starting geometry creation and design method for freeform optics," Nat. Commun. **9**, 1756 (2018).
2. T. Yang, G.-F. Jin, and J. Zhu, "Automated design of freeform imaging systems," Light: Sci. Appl. **6**, e17081 (2017).
3. G. Forbes, "Characterizing the shape of freeform optics," Opt. Express **20**, 2483–2499 (2012).
4. G. Forbes, "Fitting freeform shapes with orthogonal bases," Opt. Express **21**, 19061–19081 (2013).
5. G. Forbes, "Robust, efficient computational methods for axially symmetric optical aspheres," Opt. Express **18**, 19700–19712 (2010).
6. G. Forbes, "Shape specification for axially symmetric optical surfaces," Opt. Express **15**, 5218–5226 (2007).
7. E. Muslimov, E. Hugot, W. Jahn, S. Vives, M. Ferrari, B. Chambion, D. Henry, and C. Gaschet, "Combining freeform optics and curved detectors for wide field imaging: a polynomial approach over squared aperture," Opt. Express **25**, 14598–14610 (2017).
8. A. Bauer and J. P. Rolland, "Design of a freeform electronic viewfinder coupled to aberration fields of freeform optics," Opt. Express **23**, 28141–28153 (2015).
9. D. Ochse, "Aberration fields of anamorphic systems," Proc. SPIE **10690**, 1069018 (2018).
10. K. Fuerschbach, J. P. Rolland, and K. P. Thompson, "Theory of aberration fields for general optical systems with freeform surfaces," Opt. Express **22**, 26585–26606 (2014).
11. Y. Zhong and H. Gross, "Vectorial aberrations of biconic surfaces," J. Opt. Soc. Am. A **35**, 1385–1392 (2018).
12. Y. Zhong and H. Gross, "Initial system design method for non-rotationally symmetric systems based on gaussian brackets and nodal aberration theory," Opt. Express **25**, 10016–10030 (2017).
13. R. Winston, J. C. Miñano, P. G. Benitez, N. Shatz, and J. C. Bortz, *Nonimaging Optics* (Elsevier, 2005).
14. J. Chaves, *Introduction to Nonimaging Optics*, 2nd ed. (CRC Press, 2016).
15. W. Lin, P. Benítez, J. Miñano, J. Infante, and G. Biot, "Advances in the SMS design method for imaging optics," Proc. SPIE **8167**, 81670M (2011).
16. F. Duerr, P. Benítez, J. C. Minano, Y. Meuret, and H. Thienpont, "Analytic design method for optimal imaging: coupling three ray sets using two free-form lens profiles," Opt. Express **20**, 5576–5585 (2012).
17. J. C. Miñano, P. Benítez, W. Lin, F. Muñoz, J. Infante, and A. Santamara, "Overview of the SMS design method applied to imaging optics," Proc. SPIE **7429**, 74290C (2009).
18. J. Mendes-Lopes, P. Benítez, and J. C. Miñano, "Design of diffractive optical surfaces within the SMS design method," in *Freeform Optics* (Optical Society of America, 2015), paper FTh3B-3.
19. T. Levi-Civita, *Complementi al teorema di Malus-Dupin: nota* (Tipografia della R. Accademia dei Lincei, 1900).
20. R. G. González-Acuña and H. A. Chaparro-Romo, "General formula for bi-aspheric singlet lens design free of spherical aberration," Appl. Opt. **57**, 9341–9345 (2018).
21. R. G. González-Acuña and J. C. Guitiérrez-Vega, "Generalization of the axicon shape: the gaxicon," J. Opt. Soc. Am. A **35**, 1915–1918 (2018).
22. A. S. Glassner, *An Introduction to Ray Tracing* (Elsevier, 1989).
23. R. G. González-Acuña, "Freeform singlet lens free of spherical aberration and astigmatism," figshare (2018), https://doi.org/10.6084/m9.figshare.7476488.